Trends in Biotechnology

CellPress OPEN ACCESS

Review

Cardiac multiscale bioimaging: from nano- through micro- to mesoscales

Elen Tolstik [1,*] Stephan E. Lehnart [2,3,4,9,10] Christian Soeller [5,11] Kristina Lorenz [1,6,12,13] and Leonardo Sacconi [7,8,14,*]

Cardiac multiscale bioimaging is an emerging field that aims to provide a comprehensive understanding of the heart and its functions at various levels, from the molecular to the entire organ. It combines both physiologically and clinically relevant dimensions: from nano- and micrometer resolution imaging based on vibrational spectroscopy and high-resolution microscopy to assess molecular processes in cardiac cells and myocardial tissue, to mesoscale structural investigations to improve the understanding of cardiac (patho)physiology. Tailored super-resolution deep microscopy with advanced proteomic methods and hands-on experience are thus strategically combined to improve the quality of cardiovascular research and support future medical decision-making by gaining additional biomolecular information for translational and diagnostic applications.

Highlights

Raman spectroscopy enables label-free cardiac imaging revealing biochemical information on physiological changes induced by cardiac diseases: viability assessment of ischemic myocardium, cardiac cell analysis, and cardiac biomarker detection for early diagnosis.

Super-resolution imaging extends optical imaging to the nanometer scale to allow studying the subcellular structures (like transverse tubules and macromolecular protein clusters) that play an important role in the nanodomain physiology and pathophysiology of cardiac cells.

Large-specimen microscopy represents a fundamental tool for dissecting the complex and interconnected hierarchical organization of the heart: cellular organization can be probed across the organ opening the possibility of correlating the impact of pathologically induced structural remodeling and cardiac plasticity on heart functionality.

Cardiac imaging and microscopy

The heart is the evolutionarily evolved muscular pump able to maintain blood flow in our cardiovascular system, thanks to the coherent work of 2–3 billion excitable and contractile cells. Like bricks in a wall, cardiomyocytes (CMs) are packed alongside other cell types to form the different cardiac muscle tissues, atria and ventricles. The efficiency of cellular contraction-relaxation cycles relies on the highly ordered myofilament lattice coupled with the membrane invagination network further intercalated with dense organelles, such as mitochondria. From the cross bridges in the myofilament, which provide billions of work cycles as single linear actuators involving tension development or movement, up to the 3D organ level, a complex chain of chamber-specific contraction and relaxation movements are produced.

Understanding how cardiac contractions and relaxations occur is essential for identifying potential disease processes and mechanisms. For instance, unsynchronized electrical signals can lead to irregular heartbeats increasing life-threatening rhythm risks. Compromised mechanical function can impact the pumping ability of the heart, affecting circulation and oxygen supply. This is where the technologies mentioned in this review, such as Raman microspectroscopy or super-resolution imaging, come into play. These methods allow studying the heart at different levels, from molecules to organs, to detect subtle changes in cells, tissues, and heart chambers, thus revealing potential anomalies.

The ultimate goal of these technologies is to deepen the understanding of how the heart functions in both healthy and diseased states. This knowledge can lead to more timely and accurate diagnosis of heart conditions, for example, in biopsies [1], as well as the development of targeted treatments. In summary, analyzing the electrical and mechanical function of the heart helps to uncover the underlying causes of heart issues, guiding us toward effective strategies for maintaining cardiac health.

[1]Department of Cardiovascular Pharmacology, Translational Research, Leibniz-Institut für Analytische Wissenschaften – ISAS – e.V. Bunsen-Kirchhoff-Strasse 11, 44139 Dortmund, Germany
[2]Department of Cardiology and Pneumology, Cellular Biophysics and Translational Cardiology Section, Heart Research Center Göttingen, University Medical Center Göttingen, Georg-August University Göttingen, Robert-Koch-Strasse 42a, 37075 Göttingen, Germany
[3]Cluster of Excellence Multiscale Bioimaging: from Molecular Machines to Networks of Excitable Cells (MBExC2067), University of Göttingen, 37073 Göttingen, Germany
[4]Collaborative Research Center SFB1190 Compartmental Gates and Contact Sites in Cells, University of Göttingen, 37073 Göttingen, Germany

Cardiac imaging applying Raman spectroscopy

Raman spectroscopy (RS) helps to analyze molecular changes in cardiac samples by providing biochemical and structural information based on the diversity of molecular vibrations at all imaging levels: from subcellular organelles, CMs, or cardiac muscle to the whole organ [2]. Cardiac biomarkers in biopsies and blood can be analyzed with submicrometer resolution, high spectral selectivity, and sensitivity without the need for additional staining and the associated undesirable chemical interaction with the probe [3]. Vibrational spectroscopy relies mainly on two approaches: Raman or infrared (IR) spectroscopy, both of which provide molecule-specific spectra based on **vibrational energy levels** (see Glossary) of molecules (Boxes 1 and 2).

As the fundamental biological units of any living organism, cells yield important information about disease-related biochemical changes and molecular markers, the detection of which by Raman imaging is particularly attractive. Thus, DNA, nucleic acids, proteins, lipids and lipid droplets, lysosomes, carbohydrates, and mitochondrial activity can be assessed by Raman imaging based on their molecular composition with corresponding Raman bands and can thereby reflect the physiology of cells (Table S1 in the supplemental information online and Figure 1A,B) [3–5]. Due to specific Raman spectral profiles of porphyrin structures, the redox state of the cytochrome complex in isolated mitochondria, in CMs, and in bloodless tissue, as well as oxyhemoglobin saturation can be detected (Figure 1B) [6] and can predict cellular injury, known to be significant contributors to ischemic heart injury [7]. For example, Raman bands at 750, 1130, and around 1585 cm^{-1} can reflect a reduction of cytochromes c and b, responsible for mitochondrial respiration (Table S1 in the supplemental information online) [8], the amount of which increases with long-term ischemia, accompanied by loss of membrane potential and subsequent cell death. Ogawa and coworkers showed that the **Raman spectra** of individual CMs from healthy and infarcted myocardial regions show characteristic differences; for example, variously contribute to the functional state of mitochondria through reduced cytochrome forms (Figure 1B) [9].

Box 1. RS for biomedical application

RS is based on inelastic light scattering from biological samples (cells, tissue, blood, or urine) and provides molecular information about their biochemical structure *in vivo*, *in vitro*, or even *in situ*; for example, when examining the skin or scanning internal organs during endoscopy. When a molecule absorbs a photon, it gets excited to a higher vibrational state. Some of the photons are inelastically scattered, resulting in a frequency shift proportional to the vibrational frequency of the molecule. This shift, called Raman scattering, represents an energy difference required to excite certain molecular vibrations. The intensity of the scattered light is proportional to the population of the vibrational state and is represented as a Raman spectrum. The measured Raman spectra are unique to different functional groups within the probe and assist the customer with chemical 'fingerprints' of molecules based on their biochemical associations [4]. The Raman effect was demonstrated by two groups in 1928 and awarded a Nobel Prize to Sir C.V. Raman in 1930. However, it was not actively used in biology until breakthroughs in laser technology, spectrography, detection cameras, and the subsequent development of confocal microscopy. In the 1990s, the combination of RS with confocal microscopy enabled the application of RS in the life sciences at a level compatible with that of conventional fluorescence microscopy, with the main advantage that RS is nondestructive and label free. Therefore, there is no need for staining and pretreatment of the sample and, consequently, no sample destruction through histological examinations or time-consuming fluorescent staining. Commercial and published Raman databases (see Table S1 in the supplemental information online), or quantum mechanics calculations to estimate Raman emission are used to identify Raman bands.

Due to the structural complexity of biological specimens, biomedical spectroscopy requires extensive multivariate data analyses. Advanced chemometric methods for data pre-processing (smoothing, cosmic spike removal, baseline subtraction, and normalization) and data analysis (dimensionality reduction, statistical analyses) include the following steps: spectrum acquisition, spectral feature identification, task-oriented training, and validation of models to predict unknown samples with high quality and repeatability [86]. Multivariate data are often classified by unsupervised (principal component analysis for dimension reduction, cluster analysis, vertex component analysis, etc.) or supervised (support vector machine, linear discriminant analysis for data separation, etc.) methods, both having high computational efficiency [5].

[5]Department of Physiology, University of Bern, Bühlplatz 5, 3012 Bern, Switzerland
[6]Institute of Pharmacology and Toxicology, University of Würzburg, Versbacher Strasse 9, 97078 Würzburg, Germany
[7]Institute of Clinical Physiology, National Research Council, Rome, Italy
[8]Institute for Experimental Cardiovascular Medicine, University Freiburg, Elsässer Strasse 2q, 79110 Freiburg, Germany
[9]https://herzzentrum.umg.eu/forschung/arbeitsgruppen/zellulaere-biophysik-und-translationale-kardiologie/
[10]https://mbexc.de/about/management/#Hertha-Sponer-College-Management
[11]https://physiologie.unibe.ch/~soeller/labsite/
[12]https://www.med.uni-wuerzburg.de/pharmatoxi/startseite/
[13]https://www.isas.de/forschung/arbeitsgruppen/kardiovaskulaere-pharmakologie
[14]https://optocard.it

*Correspondence:
elen.tolstik@isas.de (E. Tolstik) and
leonardo.sacconi@cnr.it (L. Sacconi).

Box 2. Enhanced Raman spectroscopy

Enhancement of the Raman scattering process and higher spatial resolution are required for intensive bioanalytical studies and detection of disease-specific biomarkers at low concentrations [4]. Thus, SERS microscopy can be used to amplify the weak Raman scattering of biological substances by six- to eightfold using metal-based nanostructures substrates instead of standard Raman-free CaF_2 or quartz windows [27]. The interaction of the incident laser light with the nanostructures of the free-electron metals (silver or gold) creates an enhanced electric field that causes stronger Raman scattering from the molecules of interest [87]. Cells can also be incubated directly with some metal-containing enrichment solutions to achieve similar effects. It should be admitted that the nonstationary nature of the SERS signal, its fast-blinking behavior, even now leads to drawbacks in stability and reproducibility of SERS microscopy [14]. To avoid limitations in temporal resolution, fast Raman imaging techniques based on nonlinear coherent processes have been developed. Fourier transform (FT) Raman spectroscopy utilizes the combination of near-IR light and a Fourier-transformed spectrometer to acquire measurements with higher penetration depth up to a few centimeters, lower autofluorescence background and higher spectral resolution, but with limited spatial resolution in the micrometer range [2]. It is well suited for blood analyses to determine the saturation level of hemoglobin. Nonlinear CARS uses two intense laser beams with different wavelengths in the IR range, whose interaction with the material results in coherent radiation with amplified signal. Due to the IR radiation, there is a strong interference of the incident light with CO_2 and water, which makes some biological analyses not optimal. CARS is perfect for volumetric imaging in the CH range (2800–3050 cm^{-1}) with high spectral selectivity that can distinguish lipid/protein density in the sample [23]. Stimulated Raman scattering (SRS) microscopy was developed to avoid the undesirable nonresonance background of CARS and also relies on two lasers with different frequencies [4]. Resonance Raman scattering (RRS) occurs when the wavelength of the excitation laser is tuned to the light absorption band of a molecule (resonance). The closer the frequency is to the resonance, the stronger the RRS intensity. For example, in the life sciences, the absorption of aromatic molecules is often in the UV/deep UV range [8], which is commonly used to study nucleic acids, DNA/RNA, proteins, and drug–protein interactions.

Spectroscopic identification of proteins and lipids has a profound impact on cardiovascular research as an indicator of altered metabolism. RS was applied to analyze CMs; for example, to spectroscopically characterize the cardiogenic differentiation of human embryonic stem cells (ESCs) [10]; for quantitative volumetric assessment of 3D models of human induced pluripotent stem cells (hiPSCs), hiPSC-derived CMs, and adult rat ventricular CMs [11]; and to determine different lipid subtypes and protein orientations (myosin and actin filaments) in adult CMs. In endothelial cells (ECs) isolated from heart, lung, and liver in a murine model of heart failure mice, protein-specific Raman bands of amide I, tryptophan, phenylalanine, and amide III were increased compared to normal mice [5]. RS also enabled the detection of the tumor necrosis factor in ECs of various vascular beds (aorta, brain, and heart) without and with tumor necrosis factor treatment, a factor that is known to be associated with abnormal lipid accumulation [12].

In addition to cellular alteration due to pathological triggers, RS allows the identification of the cell type: isolated CMs can be identified by mitochondrial cytochrome spectra, fibroblasts by strong Raman signals from lipid droplets, and perivascular cells by a lower lipid content [13]. An RS-based analysis of cellular networks and fibrillar lamellipodia of CMs was achieved by combining surface-enhanced RS (SERS microscopy, Box 2) with stochastic reconstruction microscopy, allowing a resolution of RS microscopy down to 20 nm [14]. Overall, RS may be particularly useful for label-free discrimination of metabolic cellular statuses in certain cell types (e.g., cancer cells, CMs, and fibroblasts) [15].

RS can analyze cardiac tissue; for example, evaluate the infarct region in rat hearts after induction of ischemia (Figure 1C) [16,17]. Early subtle changes due to ischemic stress were detected by reduced Raman intensities of cytochrome, oxygenated myoglobin (Mb), and lipids. Raman hyperspectral information also allowed the discrimination between coagulation necrosis, granulation, fibrotic scar, and fibrotic tissue during infarct progression and repair (Figure 1C) [18]. In a similar context, the prediction of impending cardiac arrest in rats was demonstrated by quantification of reduced levels of electron transport chain cytochromes [6,7]. Given all these factors, RS seems suitable to detect ischemia-induced molecular changes in cardiac tissue, an analytical approach that may potentially be translated to *in vivo* analyses. With this goal, biopsies of myocardial

Glossary

Calcium indicators: fluorescent molecules that respond to the binding of Ca^{2+} ions by changing their fluorescence properties.
Diffraction-limited: refers to the theoretical limits of the spatial resolution of any optical system, due to the physics of diffraction.
Numerical aperture: a number that characterizes the range of angles over which an optical system can accept or emit light and is one of the main parameters that determines the optical resolution of a microscope.
Optogenetics: involves the expression of light-sensitive ion channels or pumps in the target cells allowing optical manipulation of transmembrane potential.
Raman spectrum: spectrum that arises from Raman (inelastic) scattering, which provides information about molecular vibrations and structural characteristics based on vibrational bonds of molecules.
Ryanodine receptor 2 (RyR2): a large intra-SR membrane ion channel that constitutes the major cellular path of calcium-induced calcium release from SR in animal CMs and other cell types.
Sarcoplasmic reticulum (SR): membrane-bound structure found within muscle cells that stores calcium ions in specialized nanodomains, the junctional SR.
Vibrational energy level: refers to the energy level associated with the vibrational motion of molecules.
Voltage-sensitive dyes: also known as potentiometric dyes, are dyes which change their spectral properties in response to transmembrane potential changes.

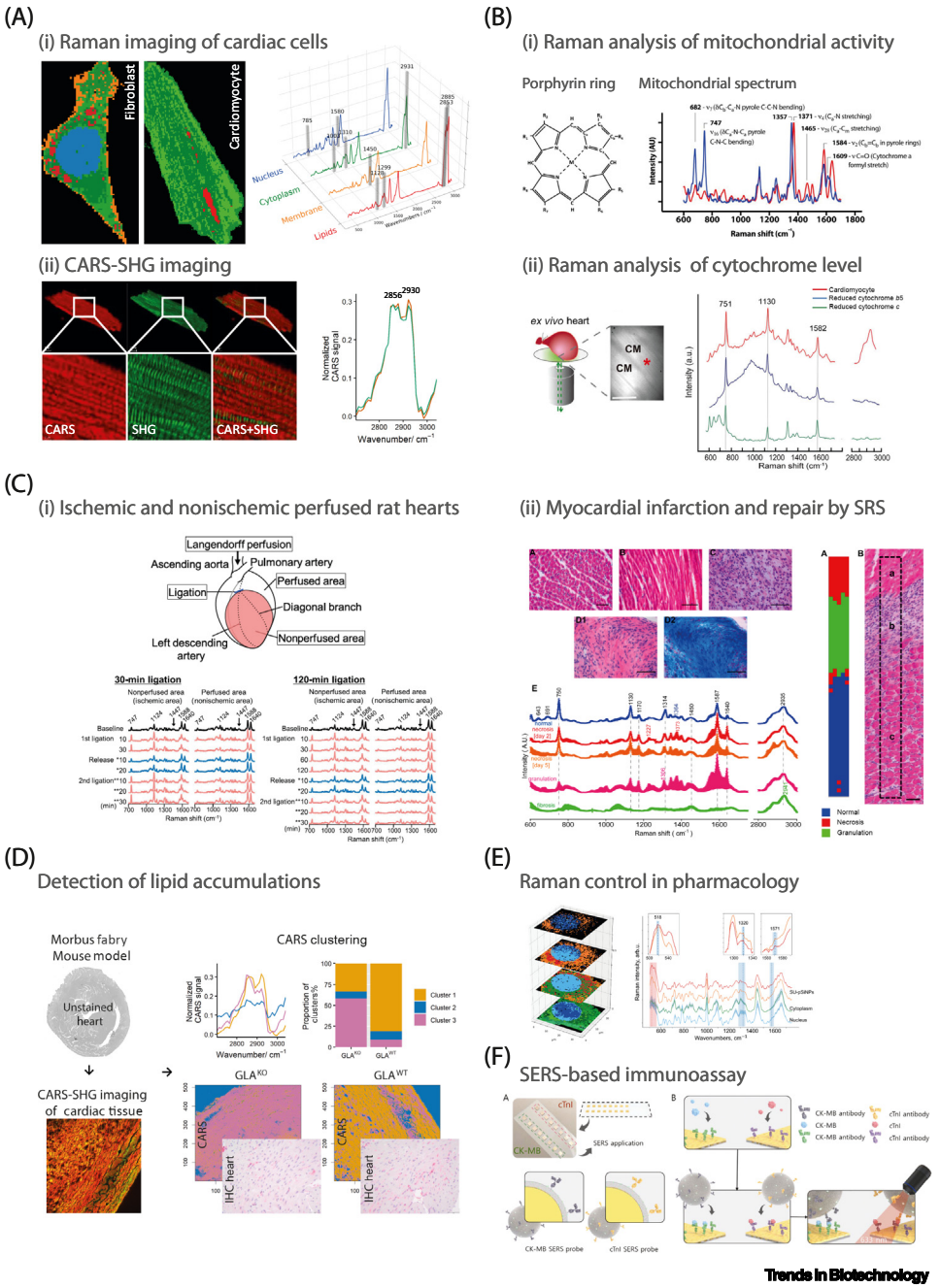

Figure 1. Raman imaging of the heart: from cardiac cells to the whole organ. (A) Spectroscopic imaging of cardiac cells from a mouse model of Fabry disease. (i) Reconstructed Raman images of a fibroblast and an isolated adult cardiomyocyte (CM) with corresponding Raman spectral clusters of nucleus, cytoplasm, membrane, and lipid associations. (ii) Coherent anti-Stokes Raman scattering (CARS)-SHG images of an isolated adult CM with corresponding CARS spectra in the CH stretching region, highlighting lipids (2850–2860 cm^{-1} wave number) and protein/lipid (2930 cm^{-1} wave number) Raman shifts for two genotypes: knockout (GLA^{KO}) and wild-type (GLA^{WT}) mice. (B) Raman analysis of mitochondrial redox states. (i) Vibrations, stretching, or bending of specific Raman bonds within the porphyrin ring and spectra for mitochondria isolated from rodent myocardium (image adapted, with permission, from [6]). (ii) Raman imaging of the cytoplasm of a representative fresh CM and heme proteins: schematic drawing of the optical setting and whole heart and Raman spectra of

(Figure legend continued at the bottom of the next page.)

infarction patients undergoing cardiac surgery were studied to identify key Raman signatures for the borders of infarcted myocardium compared to noninfarcted hearts (sensitivity of 99%) [19]. In another study, RS was applied as an alternative to the conventional electrocardiogram to examine lipid-collagen profiles in atrial biopsies of patients diagnosed with atrial fibrillation, a major risk factor for stroke [20]. Moreover, the changes in cardiac muscle, its thickening and enlargement due to cardiac hypertrophy, biomarkers, glycogen, and myofibrils could also be revealed spectroscopically [7]. Fourier transform infrared (FT-IR) spectroscopy enabled to detect early biochemical changes during heart failure development in rats based on enhanced collagen deposition, altered CM metabolism and conformational changes in tyrosine-responsive proteins (Box 2) and thereby established tyrosine and collagen Raman bands as indicators of fibrosis [21]. Similarly, FT-RS identified S-S stretching in cysteine amino acids, C-C stretching in lipids, CH_2 twisting in collagen and phospholipids, CH_3 bending modes in lipids and amino acid side chains, and amido I oscillations in proteins as major markers of ischemia reperfusion injury (Table S1 in the supplemental information online), or tyrosine and tryptophan vibrational bands as molecular markers of acute and chronic renal injury associated with the cardiorenal syndrome [22].

Since numerous proteins and lipids possess strong Raman shifts not only in the fingerprint region (<1800 cm^{-1}), but also have a sensitive contrast in the high-frequency range (>2800 cm^{-1}), a nonlinear coherent anti-Stokes Raman scattering (CARS) microscopy based on coherent amplification of the inelastic Raman signal was proved to be suited for fast volumetric imaging in the CH stretching region (Box 2) [2,3,12]. CARS microscopy revealed its potential applicability for early diagnosis of a cardiac manifestation of lysosomal storage disease, Fabry disease, in mice based on abnormal lipid accumulations in the heart (Figure 1D) [23]. CARS is also being used to investigate cholesterol and cardiovascular calcification in arteries and stenotic aortic valves [7]. Elastic fibers, collagen, lipids, β-carotene, apatite, and whitlockite minerals were determined in cross-sections of aortic tissue [24]. The technique was further improved by coupling stimulated RS with a tissue clearing technique (clearing-enhanced volumetric chemical imaging), which achieved a ten times depth extension of the label-free examination of 3D tumor spheroids based on CH vibrational modes of proteins and lipids, optimizing in-depth Raman imaging [25].

With the goal to use this analytical methodology in the clinic, Raman fiber probes have been developed and found widespread use over the past 5 years. Thus, Raman fibers for VIS and IR spectroscopy were evaluated *in vivo* for the detection of atherosclerotic plaques by monitoring

a CM obtained at the asterisk and reduced cytochromes b5 and c (image reproduced, with permission, from [9]). (C) Spectroscopic analysis of myocardial infarction regions. (i) Schematic representation of the isolated heart that is perfused retrogradely from the ascending aorta. The left ventricular wall is divided into perfused and nonperfused areas. Below: the sequential representations of averaged Raman spectra acquired from the surface of perfused rat hearts at ischemic (nonperfused) and nonischemic (perfused) areas of the 30-min and 120-min ligation models at each time point [17]. (ii) Left: evaluation of myocardial infarction and its repair by stimulated Raman scattering (SRS): histological examination (A–D) and corresponding Raman spectra (E) derived from cardiac tissues: (A) hematoxylin and eosin (H&E)-stained specimen of normal heart; (B) coagulation necrosis; (C) granulation tissue; and (D1 and D2) fibrotic scar. Right: (A) PLS-DA image; (B) H&E staining (B): (a) necrosis, (b) granulation, and (c) normal tissue [18]. Images reproduced, with permission, from the indicated references. (D) Spectroscopic imaging in lysosomal storage diseases: detection of lipid accumulation in heart tissue of mice affected by Fabry disease using CARS-SHG imaging with clustering analyses resulted in highly accurate genotype discrimination between knockout (GLA^{KO}) and wild-type (GLA^{WT}) mouse models (Image reproduced, with permission, from [23]). (E) Raman monitoring of sunitinib (SU) distribution in cardiac cells using specific Raman bands of SU and porous silicon nanoparticles (pSiNPs) used as nanocontainers for drug delivery, aiming to study drug uptake and localization, cell response, and cardiotoxicity (Image reproduced, with permission, from [93]). (F) Schematic illustration of surface-enhanced Raman spectroscopy (SERS)-based sandwich immunoassays for quantitative analysis of cardiac troponin I (cTnI) and creatine kinase MB (CK-MB) biomarkers. (A) Gold-patterned chip and SERS probes for the detection of dual biomarkers. (B) Monoclonal antibodies conjugated (cTnI and CK-MB) onto the gold-patterned chip for the capture of target antigens. SERS probe addition for the formation of sandwich immunocomplexes. Raman detection of immunocomplexes using 632.8 nm laser (Image adapted, with permission, from [27]).

the lipid–protein differentiation in plaques of aortic cross-sections of rabbits fed a high-cholesterol diet [26]. In another rodent study, fiberoptic resonance RS was tested for the prediction of cardiac dysfunction through continuous monitoring of the mitochondrial redox state [6]. This method was applied to rats under hypoxemic conditions and was able to predict the subsequent cardiac arrest with high sensitivity and specificity [6]. These techniques may possibly allow to identify early defects in oxygen delivery within the cardiac muscle.

Enhanced RS, a surface-enhanced Raman spectroscopy (SERS)-based immunoassay using gold-patterned array chips, has successfully been applied to detect cardiac troponin (cTn)I and creatine kinase (CK)-MB, two established cardiac biomarkers, in serum samples collected from patients with acute myocardial infarction (AMI) (Figure 1F and Box 2). This technique promises a significantly higher sensitivity and accuracy than current immunoassay methods [3,27]. Similarly, another highly sensitive SERS-based approach was established for the detection of heart failure biomarker brain natriuretic peptide (BNP). In this approach, functionalized nanostructures ('fingers') were used to construct Raman signals, that is, a fingerprint of BNP, and a machine learning-based algorithm was developed for a quick and accurate detection platform of myocardial infarction (acquisition time <10 s, accuracy of 98%) [28]. In a small clinical study, the application of SERS to the human urine from 87 patients with coronary artery disease (CHD) and 20 healthy humans revealed a promising correlation of the platelet-derived growth factor-BB peak, a factor closely related to CHD, with the results of the coronary angiography/cardiac congestion [29]. These studies suggest RS as a new and promising analytical method for early diagnosis of myocardial infarction or other heart diseases and possibly improved therapeutic decisions.

The limited efficiency of Raman scattering compared to fluorescence imaging, long acquisition time, and shallow penetration depth, which require direct access to the tissue sample *in vivo*, may lead to sample degradation or functional changes. Future developments in high-throughput optical elements and Raman scattering enhancement, automated AI-assisted data analysis, and improved acquisition time support widespread application of RS in the life sciences. Improvements in Raman techniques through nonlinear coherent modalities, line scanning, multifocality, and various multimodal approaches enable higher spectral and temporal sensitivity and greater penetration depth with lower resonance background and reduced autofluorescence.

High (super)-resolution cardiac imaging

High-resolution optical imaging has been relevant for cardiac imaging since the advent of confocal microscopy, if not earlier. Recent interesting applications include the label-free live-cell imaging of hPSC-derived CMs by multiphoton microscopy of autofluorescence [30] and hyperspectral imaging for label-free *in vivo* identification of myocardial scars [31]. While highly versatile, these and related methods are generally limited in spatial resolution by the diffraction limit, roughly half the wavelength of light used for imaging. The area of **diffraction-limited** microscopy applications for cardiac studies is vast, and as suggested above, new label-free approaches are becoming increasingly relevant for translational studies. In the remainder of this section, we narrow the focus on applications of super-resolution microscopy; that is, relatively recent microscopy techniques that achieve spatial resolution better than the diffraction limit by exploiting a number of optical and chemical labeling 'tricks' (Box 3).

Such improved spatial resolution is critical because many important structures of CMs are significantly smaller than the diffraction limit (~250 nm). Examples include the t tubules (with a diameter of ~200 nm in mouse CMs), the **sarcoplasmic reticulum (SR)**, which consists of a tubular network with many elements <100 nm in diameter, and the features of protein distributions that often form clusters ranging in size from 10 to several 100 nm.

Box 3. Optical super-resolution microscopy

Optical fluorescence super-resolution has seen rapid development and diversification since its introduction in the early to middle 2000s, as, for example, reviewed in [88]. In cardiac applications, STED microscopy and methods known as SMLM have been extensively applied. STED [32] is typically implemented as a scanning type of microscopy, similar to confocal microscopy. In addition to a conventional illumination beam that excites fluorochromes in the sample, STED uses a second coaligned depletion beam in a spectral regime that causes de-excitation of excited fluorochromes by a molecular process called stimulated emission. The depletion beam is focused into a donut shape with an intensity minimum at the center so that it deexcites fluorescence at the periphery of the illumination volume and by the nonlinearity of saturated depletion achieves a sharpening of the effective point spread function, in practice improving resolution to 30–80 nm. SMLM, by contrast, localizes the fluorescence from single fluorophores with a precision that is only limited by the number of photons that can be harvested, achieving resolutions between 20 and 80 nm. To form an image the location of many thousands of molecules is determined, typically achieved by taking several thousand camera frames. To enable precise localization, the images of nearby molecules must not overlap. This requires that only a few dye molecules are fluorescent in any frame, which can be achieved in several ways. When using photoactivatable dyes, a weak photoactivation beam activates few molecules at a time which are imaged and rapidly photobleached. Another approach uses photo-switching with switching buffers, where a popular method is called direct stochastic optical reconstruction microscopy (dSTORM) [89]. An alternative way to achieve single molecule 'blinking' uses synthetic DNA strands, termed DNA-PAINT [90]. All SMLM methods have in common that they produce long lists of fluorophore localizations that are then rendered into a single higher resolution image. Because many frames need to be acquired to generate a single super-resolution image, the temporal resolution of SMLM is generally low. An alternative to optical super-resolution is expansion microscopy [91]. In expansion microscopy a fixed sample is physically magnified by embedding it into a swellable gel. The expanded sample is then imaged using conventional diffraction-limited microscopy (e.g., confocal microscopy) and the resolution improvement is proportional to the physical sample expansion factor which can vary between 4 and 100× depending on the expansion protocol that is applied [92].

The range of fluorescence super-resolution microscopy (nanoscopy) techniques; that is, techniques that achieve an optical resolution better than the diffraction limit, has been ever-increasing, providing suitable approaches for almost every cardiovascular biology question (Box 3). Several flexible super-resolution techniques use a donut-shaped deexcitation laser beam (with a spot of zero intensity at the center) as the basis for deterministic nanoscopy. Early implementations of this approach improved resolution down to a few tens of nanometers or better [32]. This resolution equals the size of organelles and macromolecular machines in intact cells. Examples of this mesoscale imaging include, but are not limited to stimulated emission depletion (STED) nanoscopy of the live-cell intracellular transverse-axial-tubule-network including the width measurement of hollow luminal membrane tube sections in atrial CMs (Figure 2A); of the live-cell visualization of polyadic tubule and SR stacked superstructures in atrial CMs from Junctophilin-2 overexpressing hearts (Figure 2B), or quantitative optical capture of local Ca^{2+} signaling at the non-cardiac cochlea inner hair cell presynaptic active zones [33]; in fixed atrial myocytes from sheep with persistent atrial fibrillation the fragmentation of clusters of **ryanodine receptor (RyR)2** Ca^{2+} release channels [34]; or of the lifecycle and spatial organization of the >3 MDa protein titin at Z disks in ventricular CMs by ribosomes and proteasomes [35].

A similar spatial resolution on the order of a few tens of nanometers is provided by single-molecule localization microscopy (SMLM) techniques which localize many thousands of single fluorescence molecules over typically thousands of camera frames to assemble composite super-resolved images [36]. These techniques include photoactivated localization microscopy (PALM) and stochastic optical reconstruction microscopy (STORM), which have been used to investigate the distribution of cardiac RyR2 channels and other proteins involved in calcium handling [37,38], such as Ca^{2+}-sensitive potassium channels [39] (Figure 2C), generally using antibody staining in fixed preparations due to the relatively low time resolution of SMLM – although PALM has recently been used to measure RyR2 cluster properties in live CMs [40]. STORM has been used to investigate intercalated disk ultrastructure and molecular organization [41,42], and similarly to show that Cx43 colocalizes with dyadic RyR2 superclusters [43]. In addition, it has been used to identify a sodium channel ($Na_V1.5$) subpopulation near subjacent subsarcolemmal mitochondria [44]. Similar in concept to PALM and STORM, DNA-based point accumulation for imaging in

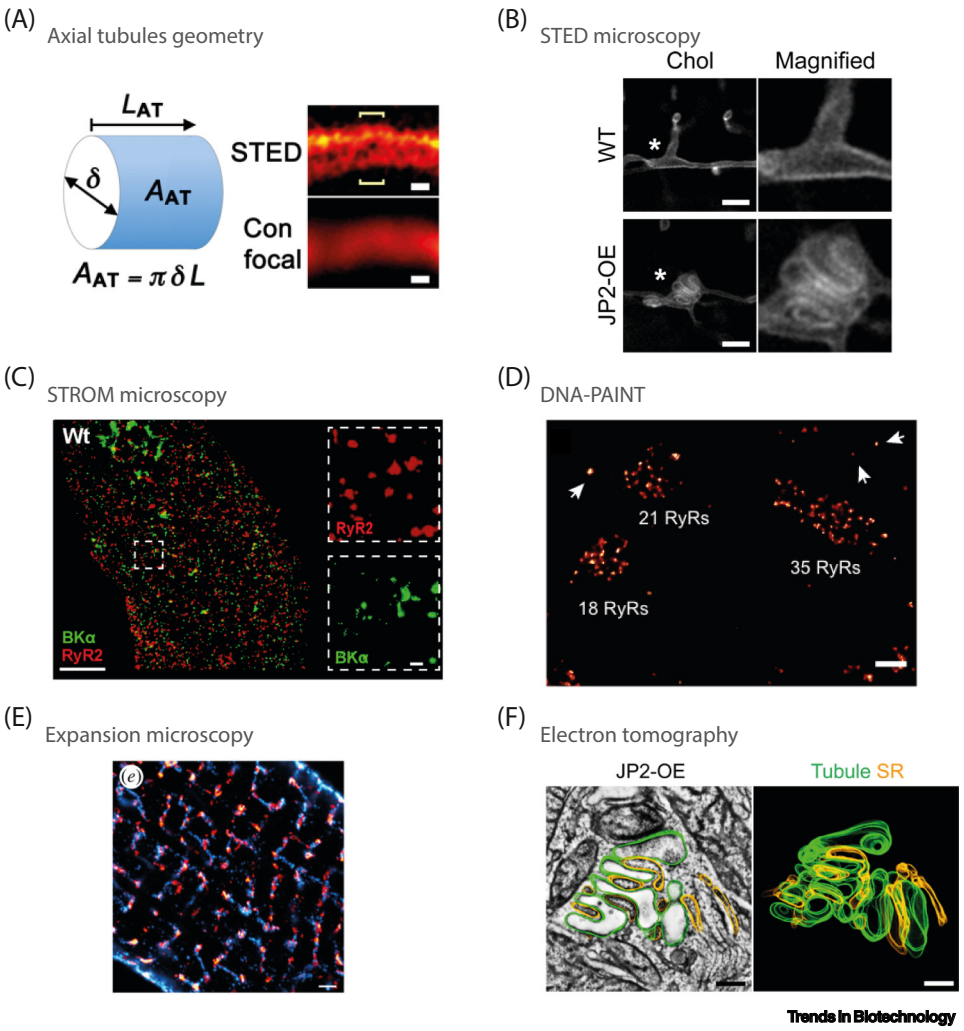

Figure 2. Super-resolution and 3D reconstruction electron tomography of cardiac cells and structures. (A) Left: cartoon conceptualizing axial tubule (AT) width (δ) measurement, length (L_{AT}), and calculated surface area (A_{AT}). Right: AT width was determined from the local stimulated emission depletion (STED) signal distribution in optical cross sections (brackets) deep inside enzymatically isolated living atrial cardiomyocytes (CMs). STED but not confocal microscopy allows for high-contrast membrane visualization and measurement of the AT width δ (293.3 ± 7.7 nm). Scale bars: 200 nm (image reproduced, with permission, from [94]). (B) WT (wild-type mouse heart) versus JP2-OE (Junctophilin-2 overexpressing mouse heart) live STED nanoscopy of cholesterol-PEG-KK114 (Chol)-stained living atrial CM. Note deep intracellular AT-associated trifurcation structures in WT versus polystacked tubule superstructures in JP2-OE CMs. Asterisks identify magnified structures. Scale bars: 1 µm (image reproduced, with permission, from [52]). (C) The image shows type 2 ryanodine receptors (RyRs) (red) and BKα channels (large conductance Ca^{2+}-activated K^+ channel pore-forming subunit) (green) imaged with ground state depletion microscopy followed by individual molecule return (GDSIM) (a variation of direct stochastic optical reconstruction microscopy; dSTORM) in a mouse smooth muscle cell. The high-resolution data allow quantifying the coassociation of RyRs and BKα. Scale bar: 3 µm, inset 300 nm (image reproduced, with permission, from [39]). (D) Clusters of RyRs were visualized with DNA-based point accumulation for imaging in nanoscale topography (DNA-PAINT) in rat ventricular myocytes. Puncta of labeling were counted and used to estimate the number of RyRs in peripheral couplings. A quantitative mode called qPAINT was also used. Scale bar: 200 nm (image reproduced, with permission, from [45]). (E) The micrograph shows expansion microscopy of an enzymically isolated rat myocytes with RyR (red) and t-tubules (cyan) stained. Note the presence of RyR clusters on longitudinal t tubules. Scale bar: 1 µm [46]. (F) JP2-OE: representative electron tomography 3D reconstruction of a tubule superstructure in JP2-OE from a high-pressure ultrarapidly cryofrozen atrial CM. Note the complex 3D tubule organization (green) and multiplexed polyadic junctional contacts with SR membranes (yellow). Scale bar: 200 nm (image reproduced, with permission, from [52]).

nanoscale topography (DNA-PAINT), a more recent type of SMLM, exploits the transient binding of diffusive, fluorescently labeled oligonucleotides/imager strands to complementary docking strands, which are in turn conjugated to a target protein, often a marker protein such as an antibody. Its advantages over PALM and STORM include effective circumvention of photobleaching and relatively large photon yields from single molecules, which improves localization precision. DNA-PAINT has been used to investigate the distribution of RyRs (Figure 2D) and its interactor Junctophilin-2 in ventricular myocytes [45].

An alternative approach which expands the sample itself, termed expansion microscopy, has been used to investigate RyR distribution in 3D in normal and CMs in a heart failure model (Figure 2E) [46]. Expansion microscopy is accessible to laboratories without advanced super-resolution microscopy equipment as the resolution enhancement is primarily achieved via suitable sample preparation protocols. A limitation is that expansion microscopy is limited to fixed samples as the chemical basis of the embedding of the sample into a swellable gel is generally not compatible with live cells.

Common to all the super-resolution approaches and applications to cardiac samples described above is that the spatial resolution generally is at a scale of 10 nm or larger; that is, not yet at the molecular level which would require resolution on the order of a single nanometer. A raft of recent refinements of super-resolution microscopies is promising to enable true molecular resolution imaging. While applications to cardiac samples have not yet been reported, we anticipate that this is only a question of time, although technical adaptions may be required to successfully image the large and spatially complex cell types found in the heart.

First in this list of advanced nanoscopy concepts is MINimal fluorescence photon FLUXes (MINFLUX), which combines the principles of STED and SMLM by localizing single molecules with an excitation light pattern in the form of a donut featuring one or more central intensity zeros [47]. As previously shown, ~2500 photons suffice to obtain a precision of <1 nm (standard deviation) in the focal plane. Even in 3D, ~2-nm precision is readily attainable by MINFLUX nanoscopy, thus resolving the spatial distribution of fluorophores at true molecular scales [47]. MINFLUX has been recently combined with DNA-PAINT using small markers such as nanobodies featuring a suitable docking strand [47,48]. A recent preprint has applied MINFLUX imaging to resolve RyR2 subunits *in situ* and shows promise to resolve the 3D orientation of protein complexes in intact VMs [49]; this illustrates the potential of truly molecular optical imaging in cardiac cells – further work will have to investigate the broader applicability to other cell types and structures in the heart.

As the ultimate molecular resolution technique, electron tomography (ET) has been applied to CMs, which allows for 3D reconstruction of subcellular volumes with a native resolution of ~1 nm^3 [50]. Combining high-pressure freezing of CMs within milliseconds after electrical excitation, snapshots of contraction-induced deformation of the intracellular nanodynamics can be captured [50]. Examples are t-tubule deformations from resting circular, contracted squeezed, to stretched elongated cross-sections [51], polyadic superstructures in Junctophilin-2 overexpressing atrial CMs (Figure 2F) [52], or RyR2 cluster changes upon phosphorylation or FKBP12/FKBP12.6 treatment [53]. During dynamic changes t-tubule cross-sections did not show a bias for high cross-section eccentricity [51].

Finally, we note that there are other ways to look at nanoscale features of myocytes, not involving optical (or electron) microscopy *per se*. Most prominent is perhaps scanning ion conductance microscopy (SICM) as pioneered by the Gorelik group in cardiac applications, which has also significant impact on signaling insights in CM [54,55]. We refer the interested reader to an existing review [56].

Large-scale cardiac imaging and manipulation

Taking these works to another order of magnitude, our capabilities of probing and manipulating the electrical dynamics across the whole heart have dramatically improved over the past years, thanks to advances in voltage and **calcium indicators**, **optogenetics** actuators [57], as well as novel optical platforms for functional imaging.

Firstly, an imaging toolkit for cardiac panoramic optical mapping was recently introduced. This comprehensive toolkit has made panoramic optical mapping more accessible to the biomedical research community at large, allowing more research groups to perform this previously highly complex approach [58]. Breakthroughs have also been made in experimental setups. A novel optical platform timely demonstrated the possibility of probing and manipulating cardiac electrical dynamics in real time by reacting acutely to ongoing cardiac waves using patterned optogenetic stimulation [59]. Optogenetic manipulation has also been utilized at a subthreshold regime, inducing a light-modulated depolarizing current with amplitudes that are too low to elicit action potentials, but are sufficient to fine-tune electrical dynamics (Figure 3A). This approach enables the induction of drifting and termination of spiral waves [60], manipulation of cardiac repolarization gradients [61], as well as increasing the magnitude of cardiac alternans [62]. Another exciting recent development is the possibility of simultaneous assessment of both electrical and mechanical dynamics in freely contracting hearts, which is achieved by disentangling fluorescence signals of the voltage sensor from mechanical deformation (Figure 3B) [63]. This approach not only enables a quantitative analysis of mechanic tissue characteristics, but intrinsically opens the possibility of studying electrical dynamics without the necessity of using pharmacological excitation–contraction uncoupling agents (Figure 3C) [64]. Although this method allows probing calcium and voltage during physiological mechanoelectrical feedback, future technical advances should also take into account the out-of-plane motion (parallel to the detection axis) and its respective correction. Recently, thanks to the development of new near-IR ratio-metric **voltage-sensitive dyes** (VSDs), the possibility of mapping electrical activity in beating hearts has been also proved in translational pig models *in vivo* [65].

A major current restriction in optical mapping systems is that electrical activity is primarily measured at the epicardial surface, which especially limits studies in larger species where transmural dynamics take place. A new generation of near-IR VSDs with deeper penetration of excitation and emission light into tissue [66], in combination with novel volumetric imaging schemes, can provide improvements in this aspect. Although volumetric voltage imaging of the whole heart has been demonstrated in zebrafish hearts [67], similar strategies would be challenging to apply to mammalian hearts given the high density of myocardial tissue and conceptually new directions are probably required. For instance, Walton and coauthors [68] demonstrated that alternating different excitation wavelengths allowed multiplexed imaging at various depths, while transillumination [69] enabled further intramural penetration with depth profiles of signal contribution differing from epifluorescence. Moreover, the subsurface volume of tissue contributing to the optical signal, known as the optical integration volume, plays a significant role in determining the dynamic signal morphology of the cardiac action potential. The size of the optical integration volume strongly influences the AP upstroke duration. The orientation of electrical wavefront propagation through the volume, concerning the imaged surface, determines the amplitude of the maximum derivative of the optical upstroke [70,71]. Recent advancements in photoacoustic imaging [72] – where the sound signature of an optical absorber is resolved in 3D across a whole heart – have provided a new perspective for the development of novel technologies for probing action potential to the underlying tissue source in a direct 3D manner.

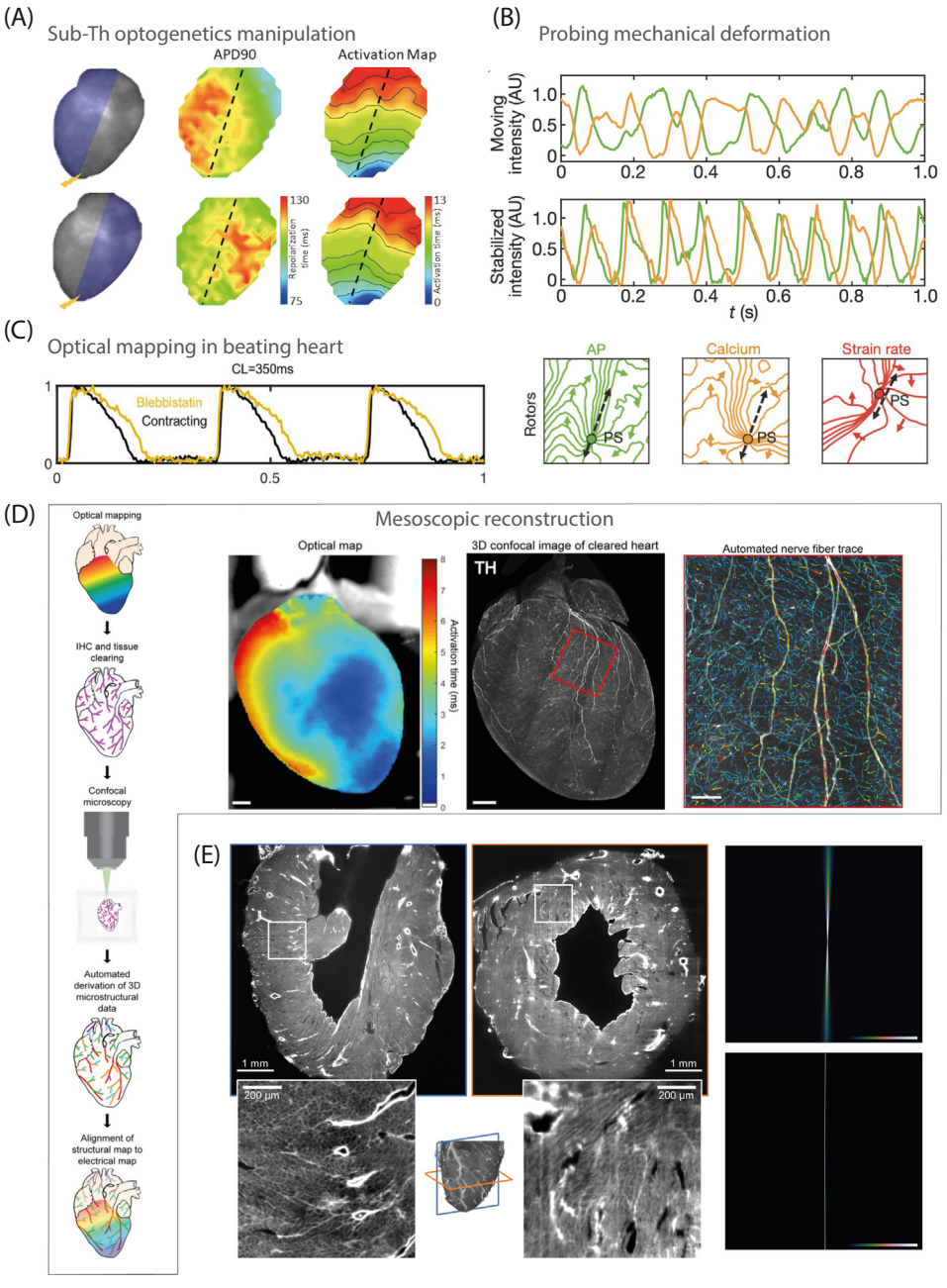

Figure 3. Mesoscopic morphofunctional imaging. (A) Imaging and manipulation of cardiac electrical dynamics using subthreshold (Sub-Th) optogenetic manipulation. ChR2 mouse hearts were electrically paced at the apex (yellow bolt symbol) while half of the heart was illuminated under a subthreshold regime. The action potential duration (APD90) and activation map correspond to the experimental condition. The broken line indicates the border between the illuminated and unilluminated region [62]. (B) Disentanglement of fluorescence signals (voltage in green, calcium in orange) from mechanical deformation using computer vision techniques. Voltage and calcium signals during ventricular fibrillation before (top) and after motion correction. The method not only overcomes the limitations imposed by motion artifacts but also enables quantitative motion analysis visualizing rotating dynamics in electrical, calcium, and mechanical activity [63]. (C) Action potential dynamics in beating versus blebbistatin-uncoupled hearts. Comparison of AP dynamics with (in yellow)

(Figure legend continued at the bottom of the next page.)

Importantly, the interpretation of cardiac electrical behaviors would benefit greatly from knowledge of the structural tissue organization, especially in the setting of pathological remodeling. However, performing large-scale imaging (in the centimeter range) at micron-scale resolution (often referred to as mesoscopic imaging) has proved challenging, and 3D reconstruction is currently accomplished by mechanical sectioning of tissue due to the inability of visible light to penetrate organs. To tackle this issue, various optical clearing techniques have been developed in recent years to create a homogeneous refractive index inside and outside the sample, minimizing scattering effects and making the sample transparent [73]. Although most of these clearing methods have been proven highly efficient in brain tissue, the heart has turned out to be comparatively difficult to treat and, up to now, there is no established clearing protocol that guarantees tissue preservation (at the organ and cellular level), high transparency, and possibility of whole-organ immunostaining, so that compromises have to be made [74]. Nevertheless, in recent years several clearing protocols have proved useful in exploring heart microvasculature architecture [75,76], CM organization [77,78], and (patho)physiological organization of the sympathetic nervous system [79]. Notably, Zhu and coauthors [80] established a powerful experimental framework for examining structure–function relationships in pathophysiological hearts by correlating optical mapping data and mesoscopic reconstruction of the sympathetic nervous system after myocardial infarction (Figure 3D).

In parallel with developing new clearing and staining protocols, the development of a new generation of optical microscopes for high-throughput mesoscopic reconstruction is also currently ongoing. To date, the best-performing technique for imaging of large organs is planar illumination microscopy [often referred to as light-sheet fluorescence microscopy (LSFM)] [81]. In short, the approach of LSFM relies on the illumination of a sample with a light sheet, coupled with a wide-field detection system positioned perpendicular to the direction of propagation of the light sheet (Box 4). By uncoupling the excitation and detection systems, it is possible to collect the signal from the entire field of view in parallel whilst maintaining effective optical sectioning provided by the localization of the excitation. However, both the thickness of the light sheet and its depth of focus depends on the **numerical aperture** (NA) of the excitation system: higher NA generates a thin light sheet, but with a limited extension of the focusing area while lower NA generates a large light sheet but with low sectioning capability.

To overcome this limitation, different strategies have been recently developed. A simple but efficient solution was found by Ding and coworkers, where an engaged depth of focus of the light sheet was achieved by applying dual-sided illumination with shifted confocal parameters [82]. Furthermore, inspired by the mesoSPIM project (mesospim.org), Giardini and coworkers [83] recently resolved single CMs and mapped them into a 3D reconstruction of whole mouse hearts in a single tomographic acquisition. In this configuration, the focal band of the light sheet is shifted in-plane through the tissue, while a rolling shutter only exposes regions of a scientific-grade CMOS camera that correspond to the axially scanned line of maximal light sheet focus in the sample, thereby producing an extraordinarily thin light sheet across the entire field of view (Figure 3E). Thanks to this implementation, the authors described the possibility of resolving single cells in three dimensions across the entire organ.

and without (in black) pharmacological excitation–contraction uncoupling agents [64]. (D) Optical mapping and tissue clearing workflow to correlate electrical and structural maps. Activation map and coregistered image of tyrosine hydroxylase-positive nerve fibers. High-magnification images of nerve-fiber tracing by computer vision, color-coded by fiber diameter [80]. (E) 3D mouse heart reconstruction. Coronal and transverse sections of a clarified heart stained with WGA conjugated to Alexa Fluor 633. The optical sectioning capability provided by mesoSPIM in combination with high tissue transparency allows the resolution of micrometric structures in the wall depth. In this configuration, the high sectioning capability is maintained across the whole field of view by the synchronization between the camera rolling shutter and the light beam position driven by the tunable lens [83]. All images reproduced, with permission, from the indicated references.

Box 4. LSFM

The basic principle of LSFM consists in illuminating the sample with a sheet of light and detecting the fluorescence signal in wide field orthogonally to the direction of propagation of the light sheet. By decoupling the excitation from the detection, it is possible to collect the fluorescence signal from the entire field of view while maintaining effective optical sectioning provided by the localization of the excitation plane. LSFM is significantly useful in volumetric imaging where the acquisition times are notably shortened compared to laser scanning techniques, such as confocal or two-photon microscopy, where all voxels have to be scanned sequentially.

This configuration allows a radial resolution determined by the detection optics and therefore expressed by Abbe's formula, while the axial resolution (optical sectioning) is dictated by the thickness of the light sheet. The light sheet is commonly realized dynamically by using a galvanometric mirror that scans at high speed the excitation ray into the converging lens, thus translating the light beam throughout the illumination plane and generating a virtual sheet of light. The focused beam has therefore a simple Gaussian profile (Figure I) characterized by the following thickness:

$$w(z) = w_0\sqrt{1 + \left(\frac{z}{z_R}\right)^2}$$

with:

$$z_R = \frac{nw_0^2 n}{\lambda}$$

where z is the propagation axis, the parameter w_0 represents the minimum thickness of the light sheet (called beam waist), n is the refractive index where the sample is immersed, and λ the excitation wavelength.

The distance (b in Figure I) between the two points $\pm z_R$ is called the depth of focus of the beam and represents the limit in which the thickness of the light sheet can be considered uniform, defining the maximum field of view.

Importantly, b depends on w_0; therefore, thin light sheet has limited extension of the focusing zone. On the other hand, large extension of the light sheet can achieve only with low sectioning power, compromising the possibility of analyzing 3D structures with an isometric resolution.

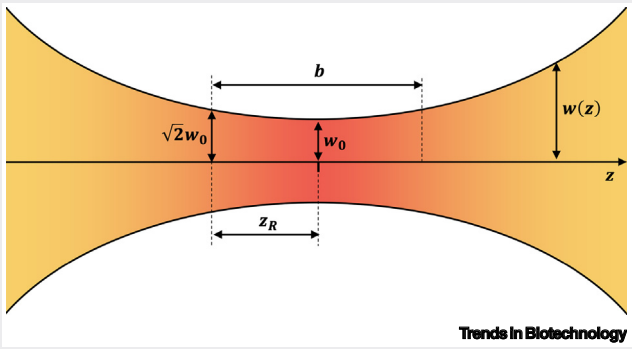

Figure I. Spatial profile (beam width) of a focused Gaussian beam.

Outstanding questions

The quantitative and qualitative biochemical information obtained by RS from the untreated heart biopsy can be well correlated with the pathological examination as a preliminary molecular assessment. However, the shallow penetration depth *in vivo* and thus the need for direct access to the tissue sample, the undesirable presence of blood for imaging, the long acquisition time and the low signal of inelastic Raman scattering compared to tissue autofluorescence lead to limitations in biomedical applications. What improvements to RS are needed for the successful adoption of Raman imaging in the life sciences? Could the amplification of Raman signals and the automated use of machine learning algorithms help optimize and improve data analysis?

In parallel, super-resolution microscopy has been proven efficient in providing ultrastructural and molecular information in living cells. However, can high-resolution optical imaging techniques that approach the single-nanometer scale be successfully applied in tissues? Will high spatial resolution imaging become compatible with the high temporal resolution required to capture fast dynamic processes such as those during calcium signaling?

Moving from nano- to meso-scales, how can super-resolution be efficiently integrated into imaging modalities with larger fields of view? How feasible will data management and analysis be? In general, how important will machine learning become in providing automated microscopy, as well as improved analysis and segmentation for cardiac applications at various scales, and how quickly will this transformation occur?

Lastly, even if not optically based, cardiac imaging has also made significant progress in whole-heart microscale structural imaging for large mammalian species using microCT [84,85]. In this context, new air-drying tissue pretreatment regimes have been developed, leading to a reduction in tissue density and stabilization in the air for optimized X-ray transmission and high-contrast imaging.

Concluding remarks and future perspectives

We aimed to provide a comprehensive, scientific overview of the current cutting-edge imaging techniques in cardiovascular research, their applications in biology and potential for translation into bio- and medical technologies. The review summarizes how those imaging tools help gain

better insights into cardiac morphology and molecular alterations, cardiac function and the translation of these insights into new approaches for diagnosis, treatment, and management of heart disease. It also discusses the limitations of both live and fixed sampling and the difficulties of the aforementioned techniques.

Raman imaging identifies molecular alterations in biochemical compositions of cells and tissue of the heart in a label-free way that is attractive for detection of cardiac hypertrophy. Blood analysis by RS allows quick detection of AMI. SERS microscopy enables distinguishing low concentrations of biochemicals and analytes. Achieving high-speed nanometer-scale Raman imaging holds the potential of a breakthrough in biological imaging. Combinations such as SERS and high-resolution microscopy, SERS–STORM microscopy, optical tweezers for single cell localization, Raman-activated droplet sorting, deep tissue analyses by tissue clearance, portable Raman fiber probes – all support the implementation of RS in daily clinical practice, providing physicians with not only visual but also molecular-based information from the critical tissue area.

Super-resolution microscopy techniques have clearly become important tools in studying cardiovascular biology. With the recent advent of true molecular imaging at the single nanometer resolution level, we will likely soon see applications of these cutting-edge techniques in CM preparations, where many molecular questions still await answers. In this regard, a technique called one-nanometer expansion (ONE) microscopy [45] was recently established by combining X10 expansion microscopy with a type of super-resolution microscopy based on determining higher-order statistical analysis of temporal fluctuations measured in a series of camera frames, known as super-resolution radial fluctuations (SRRFs) [46]. ONE can be implemented using conventional confocal or epifluorescence microscopes and achieves 1 nm or better resolutions across different samples and color channels, using labeled immunoglobulins [45].

Finally, extended field-of-view and spatial resolution have recently been achieved, thanks to the new generation of mesoscopic morphofunctional imaging operating at whole tissue level. Hence, current advances in imaging make the development of an ideal experimental framework to dissect cardiac electrophysiology increasingly feasible. In a futuristic scenario, transmembrane potentials and calcium release can be recorded in 3D, while simultaneously tracking the movement of a freely beating heart. In addition to the investigation of electrophysiological characteristics, novel advances in imaging methods and tissue preparations can be combined with novel software strategies for analysis, processing, and correlation of structural and functional data at single-cell resolution. Together, these developments will lead to further understanding mechanisms driving, for example, arrhythmias, while aiding the development of novel therapies (see Outstanding questions).

Acknowledgments

This study was supported by the Federal Ministry of Education and Research [Bundesministerium für Bildung und Forschung, BMBF; ChinValue (03INT703AB)], Ministry of Culture and Science of the State of North Rhine-Westphalia, ERK-Casting (16GW0262K), the Swiss National Science Foundation (310030_208109), the European Union's Horizon 2020 research and innovation program under grant agreement No 952166 (REPAIR); Fondazione CR Firenze, SALUS project, the Deutsche Forschungsgemeinschaft's Collaborative Research Centers SFB1425 (DFG #422681845), SFB1525 (#453989101), SFB1190 to SEL (project P03) and SFB/TR 296 (#424957847), the Drug Discovery Hub Dortmund (DDHD) and was supported under Germany's Excellence Strategy (EXC2067/1-390729940).

Declarations of interest

No interests are declared.

Supplemental information

Supplemental information associated with this article can be found online https://doi.org/10.1016/j.tibtech.2023.08.007.

References

1. Brandenburg, S. *et al.* (2022) Direct proteomic and high-resolution microscopy biopsy analysis identifies distinct ventricular fates in severe aortic stenosis. *J. Mol. Cell. Cardiol.* 173, 1–15
2. Kato, R. *et al.* (2022) High-sensitivity hyperspectral vibrational imaging of heart tissues by mid-infrared photothermal microscopy. *Anal. Sci.* 38, 1497–1503
3. Chaichi, A. *et al.* (2018) Raman spectroscopy and microscopy applications in cardiovascular diseases: from molecules to organs. *Biosens. Basel* 8, 107
4. Lee, K.S. *et al.* (2021) Raman microspectroscopy for microbiology. *Nat. Rev. Methods Primers* 1, 80
5. Tott, S. *et al.* (2021) Raman imaging-based phenotyping of murine primary endothelial cells to identify disease-associated biochemical alterations. *Biochim. Biophys. Acta Mol. Basis Dis.* 1867, 166180
6. Perry, D.A. *et al.* (2017) Responsive monitoring of mitochondrial redox states in heart muscle predicts impending cardiac arrest. *Sci. Transl. Med.* 9, eaan0117
7. Kumamoto, Y. *et al.* (2018) Label-free molecular imaging and analysis by raman spectroscopy. *Acta Histochem. Cytochem.* 51, 101–110
8. Kawata, S. *et al.* (2017) Nano-Raman scattering microscopy: resolution and enhancement. *Chem. Rev.* 117, 4983–5001
9. Ogawa, M. *et al.* (2009) Label-free biochemical imaging of heart tissue with high-speed spontaneous Raman microscopy. *Biochem. Bioph. Res. Co.* 382, 370–374
10. Pascut, F.C. *et al.* (2013) Non-invasive label-free monitoring the cardiac differentiation of human embryonic stem cells in-vitro by Raman spectroscopy. *Biochim. Biophys. Acta Gen. Subj.* 1830, 3517–3524
11. Kallepitis, C. *et al.* (2017) Quantitative volumetric Raman imaging of three dimensional cell cultures. *Nat. Commun.* 8, 14843
12. Radwan, B. *et al.* (2020) Labeled vs. label-free raman imaging of lipids in endothelial cells of various origins. *Molecules* 25, 5752
13. Tott, S. *et al.* (2018) Raman spectroscopic features of primary cardiac microvascular endothelial cells (CMECs) isolated from the murine heart. *Analyst* 143, 6079–6086
14. Ayas, S. *et al.* (2013) Label-free nanometer-resolution imaging of biological architectures through surface enhanced Raman scattering. *Sci. Rep.* 3, 2624
15. Surmacki, J.M. *et al.* (2018) Raman micro-spectroscopy for accurate identification of primary human bronchial epithelial cells. *Sci. Rep.* 8, 12604
16. Ohira, S. *et al.* (2017) Label-free detection of myocardial ischaemia in the perfused rat heart by spontaneous Raman spectroscopy. *Sci. Rep.* 7, 42401
17. Ikemoto, K. *et al.* (2021) Raman spectroscopic assessment of myocardial viability in Langendorff-perfused ischemic rat hearts. *Acta Histochem. Cytochem.* 54, 65–72
18. Nishiki-Muranishi, N. *et al.* (2014) Label-free evaluation of myocardial infarction and its repair by spontaneous Raman spectroscopy. *Anal. Chem.* 86, 6903–6910
19. Yamamoto, T. *et al.* (2018) Label-free evaluation of myocardial infarct in surgically excised ventricular myocardium by Raman spectroscopy. *Sci. Rep.* 8, 14671
20. Parlatan, U. *et al.* (2022) Atrial fibrillation designation with micro-Raman spectroscopy and scanning acoustic microscope. *Sci. Rep.* 12, 6461
21. Tombolesi, N. *et al.* (2022) Early cardiac-chamber-specific fingerprints in heart failure with preserved ejection fraction detected by FTIR and Raman spectroscopic techniques. *Sci. Rep.* 12, 3440
22. Nepomuceno, G. *et al.* (2021) Tyrosine and Tryptophan vibrational bands as markers of kidney injury: a renocardiac syndrome induced by renal ischemia and reperfusion study. *Sci. Rep.* 11, 15036
23. Tolstik, E. *et al.* (2022) CARS Imaging advances early diagnosis of cardiac manifestation of Fabry disease. *Int. J. Mol. Sci.* 23, 5345
24. You, A.Y.F. *et al.* (2017) Raman spectroscopy imaging reveals interplay between atherosclerosis and medial calcification in the human aorta. *Sci. Adv.* 3, e1701156
25. Wei, M. *et al.* (2019) Volumetric chemical imaging by clearing-enhanced stimulated Raman scattering microscopy. *Proc. Natl. Acad. Sci. U. S. A.* 116, 6608–6617
26. Lattermann, A. *et al.* (2013) Characterization of atherosclerotic plaque depositions by Raman and FTIR imaging. *J. Biophotonics* 6, 110–121
27. Cheng, Z.Y. *et al.* (2019) SERS-based immunoassay using gold-patterned array chips for rapid and sensitive detection of dual cardiac biomarkers. *Analyst* 144, 6533–6540
28. Liu, Z. *et al.* (2023) Ultrafast early warning of heart attacks through plasmon-enhanced Raman spectroscopy using collapsible nanofingers and machine learning. *Small* 19, e2204719
29. Yang, H. *et al.* (2018) Noninvasive and prospective diagnosis of coronary heart disease with urine using surface-enhanced Raman spectroscopy. *Analyst* 143, 2235–2242
30. Qian, T.C. *et al.* (2021) Label-free imaging for quality control of cardiomyocyte differentiation. *Nat. Commun.* 12, 4580
31. Swift, L.M. *et al.* (2018) Hyperspectral imaging for label-free in vivo identification of myocardial scars and sites of radiofrequency ablation lesions. *Heart Rhythm.* 15, 564–575
32. Klar, T.A. *et al.* (2000) Fluorescence microscopy with diffraction resolution barrier broken by stimulated emission. *Proc. Natl. Acad. Sci. U. S. A.* 97, 8206–8210
33. Neef, J. *et al.* (2018) Quantitative optical nanophysiology of Ca^{2+} signaling at inner hair cell active zones. *Nat. Commun.* 9, 290
34. Macquaide, N. *et al.* (2015) Ryanodine receptor cluster fragmentation and redistribution in persistent atrial fibrillation enhance calcium release. *Cardiovasc. Res.* 108, 387–398
35. Rudolph, F. *et al.* (2019) Resolving titin's lifecycle and the spatial organization of protein turnover in mouse cardiomyocytes. *Proc. Natl. Acad. Sci. U. S. A.* 116, 25126–25136
36. Lelek, M. *et al.* (2021) Single-molecule localization microscopy. *Nat. Rev. Methods Primers* 1
37. Jayasinghe, I. *et al.* (2018) Shining new light on the structural determinants of cardiac couplon function: insights from ten years of nanoscale microscopy. *Front. Physiol.* 9, 1472
38. Dixon, R.E. (2021) Nanoscale organization, regulation, and dynamic reorganization of cardiac calcium channels. *Front. Physiol.* 12, 810408
39. Pritchard, H.A.T. *et al.* (2018) Nanoscale remodeling of ryanodine receptor cluster size underlies cerebral microvascular dysfunction in Duchenne muscular dystrophy. *Proc. Natl. Acad. Sci. U. S. A.* 115, E9745–E9752
40. Hou, Y. *et al.* (2023) Live-cell photoactivated localization microscopy correlates nanoscale ryanodine receptor configuration to calcium sparks in cardiomyocytes. *Nat. Cardiovasc. Res.* 2, 251–267
41. Bogdanov, V. *et al.* (2021) Distributed synthesis of sarcolemmal and sarcoplasmic reticulum membrane proteins in cardiac myocytes. *Basic Res. Cardiol.* 116, 63
42. Veeraraghavan, R. *et al.* (2016) Potassium channels in the Cx43 gap junction perinexus modulate ephaptic coupling: an experimental and modeling study. *Pflug Arch. Eur. J. Phy.* 468, 1651–1661
43. De Smet, M.A. *et al.* (2021) Cx43 hemichannel microdomain signaling at the intercalated disc enhances cardiac excitability. *J. Clin. Invest.* 131, e137752
44. Perez-Hernandez, M. *et al.* (2021) Structural and functional characterization of a Na(v)1.5-mitochondrial couplon. *Circ. Res.* 128, 419–432
45. Jayasinghe, I. *et al.* (2018) True molecular scale visualization of variable clustering properties of ryanodine receptors. *Cell Rep.* 22, 557–567
46. Sheard, T.M.D. *et al.* (2022) Three-dimensional visualization of the cardiac ryanodine receptor clusters and the molecular-scale fraying of dyads. *Philos. Trans. R. Soc. Lond. Ser. B Biol. Sci.* 377, 20210316
47. Ostersehlt, L.M. *et al.* (2022) DNA-PAINT MINFLUX nanoscopy. *Nat. Methods* 19, 1072–1075
48. Strauss, S. and Jungmann, R. (2020) Up to 100-fold speed-up and multiplexing in optimized DNA-PAINT. *Nat. Methods* 17, 789–791
49. Clowsley, A.H. *et al.* (2023) Analysis of RyR2 distribution in HEK293 cells and mouse cardiac myocytes using 3D MINFLUX microscopy. *bioRxiv* Published online July 28, 2023 https://doi.org/10.1101/2023.07.26.550636
50. Kohl, P. *et al.* (2022) Electron microscopy of cardiac 3D nanodynamics: form, function, future. *Nat. Rev. Cardiol.* 19, 607–619

51. Rog-Zielinska, E.A. *et al.* (2021) Beat-by-beat cardiomyocyte T-tubule deformation drives tubular content exchange. *Circ. Res.* 128, 203–215
52. Brandenburg, S. *et al.* (2019) Junctophilin-2 expression rescues atrial dysfunction through polyadic junctional membrane complex biogenesis. *JCI Insight* 4, e127116
53. Asghari, P. *et al.* (2020) Cardiac ryanodine receptor distribution is dynamic and changed by auxiliary proteins and post-translational modification. *eLife* 9, e51602
54. Nikolaev, V.O. *et al.* (2010) Beta2-adrenergic receptor redistribution in heart failure changes cAMP compartmentation. *Science* 327, 1653–1657
55. Schmid, E. *et al.* (2015) Cardiac RKIP induces a beneficial beta-adrenoceptor-dependent positive inotropy. *Nat. Med.* 21, 1298–1306
56. Miragoli, M. *et al.* (2011) Scanning ion conductance microscopy: a convergent high-resolution technology for multi-parametric analysis of living cardiovascular cells. *J. R. Soc. Interface* 8, 913–925
57. Entcheva, E. and Kay, M.W. (2021) Cardiac optogenetics: a decade of enlightenment. *Nat. Rev. Cardiol.* 18, 349–367
58. Gloschat, C. *et al.* (2018) RHYTHM: an open source imaging toolkit for cardiac panoramic optical mapping. *Sci. Rep.* 8, 2921
59. Scardigli, M. *et al.* (2018) Real-time optical manipulation of cardiac conduction in intact hearts. *J. Physiol.* 596, 3841–3858
60. Hussaini, S. *et al.* (2021) Drift and termination of spiral waves in optogenetically modified cardiac tissue at sub-threshold illumination. *eLife* 10, e59954
61. Marchal, G.A. *et al.* (2023) Optogenetic manipulation of cardiac repolarization gradients using sub-threshold illumination. *Front. Physiol.* 14, 1167524
62. Biasci, V. *et al.* (2022) Optogenetic manipulation of cardiac electrical dynamics using sub-threshold illumination: dissecting the role of cardiac alternans in terminating rapid rhythms. *Basic Res. Cardiol.* 117, 25
63. Christoph, J. *et al.* (2018) Electromechanical vortex filaments during cardiac fibrillation. *Nature* 555, 667–672
64. Kappadan, V. *et al.* (2020) High-resolution optical measurement of cardiac restitution, contraction, and fibrillation dynamics in beating vs. blebbistatin-uncoupled isolated rabbit hearts. *Front. Physiol.* 11, 464
65. Lee, P. *et al.* (2019) In vivo ratiometric optical mapping enables high-resolution cardiac electrophysiology in pig models. *Cardiovasc. Res.* 115, 1659–1671
66. Yan, P. *et al.* (2023) Near infrared voltage sensitive dyes based on chromene electron donors. *Proc. Natl. Acad. Sci. U. S. A.* 120, e2305093120
67. Sacconi, L. *et al.* (2022) KHz-rate volumetric voltage imaging of the whole Zebrafish heart. *Biophys. Rep. (N. Y.)* 2, 100046
68. Walton, R.D. *et al.* (2010) Dual excitation wavelength epifluorescence imaging of transmural electrophysiological properties in intact hearts. *Heart Rhythm.* 7, 1843–1849
69. Baxter, W.T. *et al.* (2001) Visualizing excitation waves inside cardiac muscle using transillumination. *Biophys. J.* 80, 516–530
70. Hyatt, C.J. *et al.* (2005) Optical action potential upstroke morphology reveals near-surface transmural propagation direction. *Circ. Res.* 97, 277–284
71. Walton, R.D. *et al.* (2012) Extracting surface activation time from the optically recorded action potential in three-dimensional myocardium. *Biophys. J.* 102, 30–38
72. Ozsoy, C. *et al.* (2021) Ultrafast four-dimensional imaging of cardiac mechanical wave propagation with sparse optoacoustic sensing. *Proc. Natl. Acad. Sci. U. S. A.* 118
73. Richardson, D.S. *et al.* (2021) Tissue clearing. *Nat. Rev. Methods Primers* 1, 84
74. Olianti, C. *et al.* (2022) Optical clearing in cardiac imaging: a comparative study. *Prog. Biophys. Mol. Biol.* 168, 10–17
75. Vinegoni, C. *et al.* (2020) Fluorescence microscopy tensor imaging representations for large-scale dataset analysis. *Sci. Rep.* 10, 5632
76. Nehrhoff, I. *et al.* (2017) Looking inside the heart: a see-through view of the vascular tree. *Biomed. Opt. Express* 8, 3110–3118
77. Giardini, F. *et al.* (2021) Quantification of myocyte disarray in human cardiac tissue. *Front. Physiol.* 12, 750364
78. Wang, Z. *et al.* (2018) Imaging transparent intact cardiac tissue with single-cell resolution. *Biomed. Opt. Express* 9, 423–436
79. Yokoyama, T. *et al.* (2017) Quantification of sympathetic hyperinnervation and denervation after myocardial infarction by three-dimensional assessment of the cardiac sympathetic network in cleared transparent murine hearts. *PLoS One* 12, e0182072
80. Zhu, C. *et al.* (2022) High-resolution structure-function mapping of intact hearts reveals altered sympathetic control of infarct border zones. *JCI Insight* 7, e153913
81. Pera, M.F. (2011) The proteomes of native and induced pluripotent stem cells. *Nat. Methods* 8, 807–808
82. Ding, Y. *et al.* (2017) Light-sheet fluorescence imaging to localize cardiac lineage and protein distribution. *Sci. Rep.* 7, 42209
83. Giardini, F. *et al.* (2021) Mesoscopic optical imaging of whole mouse heart. *J. Vis. Exp.* Published online October 14, 2021 https://doi.org/10.3791/62795
84. Pallares-Lupon, N. *et al.* (2023) Optimizing large organ scale micro computed tomography imaging in pig and human hearts using a novel air-drying technique. *bioRxiv* Published online July 29, 2021. https://doi.org/10.1101/2021.07.29.454121
85. Pallares-Lupon, N. *et al.* (2022) Tissue preparation techniques for contrast-enhanced micro computed tomography imaging of large mammalian cardiac models with chronic disease. *J. Vis. Exp.* Published online February 8, 2022. https://doi.org/10.3791/62909
86. Huang, J. *et al.* (2020) Vibrational spectroscopy as a powerful tool for follow-up immunoadsorption therapy treatment of dilated cardiomyopathy - a case report. *Analyst* 145, 486–496
87. Panneerselvam, R. *et al.* (2017) Surface-enhanced Raman spectroscopy: bottlenecks and future directions. *Chem. Commun. (Camb.)* 54, 10–25
88. Fornasiero, E.F. and Opazo, F. (2015) Super-resolution imaging for cell biologists: concepts, applications, current challenges and developments. *BioEssays* 37, 436–451
89. van de Linde, S. *et al.* (2011) Direct stochastic optical reconstruction microscopy with standard fluorescent probes. *Nat. Protoc.* 6, 991–1009
90. Schnitzbauer, J. *et al.* (2017) Super-resolution microscopy with DNA-PAINT. *Nat. Protoc.* 12, 1198–1228
91. Chen, F. *et al.* (2015) Optical imaging. Expansion microscopy. *Science* 347, 543–548
92. Wassie, A.T. *et al.* (2019) Expansion microscopy: principles and uses in biological research. *Nat. Methods* 16, 33–41
93. Tolstik, E. *et al.* (2022) Raman and fluorescence micro-spectroscopy applied for the monitoring of sunitinib-loaded porous silicon nanocontainers in cardiac cells. *Front. Pharmacol.* 13, 962763
94. Brandenburg, S. *et al.* (2016) Axial tubule junctions control rapid calcium signaling in atria. *J. Clin. Invest.* 126, 3999–4015